ENHANCED CAUSAL DIGRAPH REASONING FOR FAULT DIAGNOSIS WITH APPLICATION ON THE PAPER MACHINE SHORT CIRCULATION PROCESS

Hui Cheng, Mats Nikus, Sirkka-Liisa Jämsä-Jounela

Helsinki University of Technology
Laboratory of Process Control and Automation
Kemistintie 1, FI-02150 HUT, Finland

Abstract: This paper presents an enhanced dynamic causal digraph reasoning method for fault diagnosis and its application to the short circulation process of a paper machine. In order to improve the isolation capability of the original method, an inference mechanism between the arcs of the graph is proposed to locate process faults on the arcs. Application of the proposed method to the paper machine short circulation process is presented at the end of the paper. The results show that the proposed method is able to identify the responsible arcs when the system is affected by a process fault.

Keywords: Causal Digraph, Paper Machine, CUSUM

1. INTRODUCTION

Research in the field of fault diagnosis has been very active since the 70s. In order to meet the demands from industry concerning quality, efficiency and safety, numerous fault diagnosis methods have been developed. Of these, causal model based methods have attracted considerable attention since they were first developed by Iri et al (1979). As a modelling method, the causal model is able to describe the system behaviour in terms of cause-effect relationships between the entities of a system (Fagarasan et al., 2004), which is represented by a directed graph. The causal models can be used for many different purposes, such as simulation (Leyval, Gentil & Feray-Beaumont, 1994) and fault diagnosis (Montmain & Gentil, 2000).

Since Iri et al. (1979) introduced the Signed Directed Graph (SDG), the simplest causal digraph method, into the field of process fault diagnosis, it has made remarkable progress and been the most popular causal model based method for process fault diagnosis. In order to alleviate the problem with spurious results, fuzzy logic was used by Shih and Lee (1995) to represent both the variables and the relations in the causal digraph. However the method itself still remained static. Another big improvement of the causal digraph was the introduction of the piece-wise linear transfer functions (QTF) by Leyval et al. (1994). The used simplified transfer function provides dynamic information. With the introduction of the QTF a new reasoning method for diagnosis purposes was based on residuals was needed. Recently more quantitative models, such as difference-algebraic equations (Montmain & Gentail, 2000) have been used in causal digraph to further improve the diagnosis results.

As reported by Montmain and Gentil (2000) and Fagarasan et al. (2004), the dynamic causal digraph method is able to manage different types of fault: sensor, actuator and process faults. However, the ability of the dynamic causal digraph method to handle process faults is limited. The method assumes that a primary fault is a change in a variable (a node in the digraph) rather than a change in the consistency between the variables (an arc in the digraph). In industrial applications, however, it is usually required to know the corresponding faulty process components. This requirement can be met in the case of measurement faults, since the nodes in the digraph model represent the sensor of the process, while faulty nodes alone cannot provide enough information to identify the faulty process components corresponding to the arcs in the digraph. One important topic is therefore to locate the responsible arcs, and furthermore an inference mechanism between arcs has been developed by the authors to achieve this aim.

The paper is organized as follows. In Chapter 2 the enhanced dynamic causal reasoning method is proposed including the CUSUM method and the inference mechanism between arcs. In Chapter 3 the short circulation process of a paper machine and the simulation environment are introduced. Two different fault scenarios, description of the experiment and the fault diagnosis results for each fault scenario are given in Chapter 4, followed by the conclusions in Chapter 5.

2. ENHANCED DYNAMIC CAUSAL DIGRAPH METHOD

An enhanced dynamic causal digraph method designed to locate the process fault on the arcs is proposed in this chapter. The proposed method

performs the fault detection and isolation in four steps as follows

1. Generate the global (*GR*) and local residuals (*LR*)
2. Detect a possible abnormality in the residual signals using the CUSUM method
3. For the variables in the detection set, locate the primary fault and identify its nature by means of the fault isolation and nature rules
4. In case of a process fault, an additional inference step between arcs is performed in order to locate the fault on the responsible arc(s)

Discrete-time state space models are used to describe the cause-effect relationships between variables in the causal models.

2.1 Residual generation with the dynamic causal model

The dynamic causal digraph produces two kinds of residual to be used in fault detection and isolation: global and local residuals. The global residual is produced for the purpose of fault detection by the difference between the measurement and the global propagation value:

$$GR(Y) = Y(k) - \hat{Y}(k) \quad (1)$$

where $Y(k)$ is the measurement and $\hat{Y}(k)$ is the global propagation value obtained by

$$\begin{aligned} \hat{X}(k+1) &= A\hat{X}(k) + B\hat{U}(k) \\ \hat{Y}(k) &= C\hat{X}(k) \end{aligned} \quad (2)$$

where $\hat{U}(k) = \left[\hat{U}_1(k),....\hat{U}_n(k)\right]^T$ is the lagged global propagation value from the predecessors in the graph model, $\hat{X}(0) = x_0$ is the initial state, and n denotes the number of inputs for variable *Y*.

The local residuals are subcategorized into three types: individual local residuals (*ILR*), multiple local residuals (*MLR*) and total local residuals (*TLR*).

The individual local residual is produced by taking the difference between the measurement and the local propagation value with only one measured input, while all the others are propagation values from the parent nodes.

$$\begin{aligned} X'(k+1) &= AX'(k) + BU(m,k) \\ Y'(k) &= CX'(k) \\ ILR_Y(m) &= Y(k) - Y'(k) \end{aligned} \quad (3)$$

where $U(m,k) = \left[\hat{U}_1(k),...U_m(k),...\hat{U}_n(k)\right]^T$, $\hat{U}_i(k)$ is the global propagated value from the predecessors, and $i \neq m$, $U_m(k)$ is the measurement for the parent node and $X'(0) = x_0$ is the initial state.

Similarly, the $MLR_Y(P)$ is produced with input $U(P,k) = \left[\hat{U}_1(k),..U_j(k),..\hat{U}_n(k)\right]^T$, $j \in P$, P is the set of subscripts of the predecessors which use the measurement as an input. The $TLR(Y)$ is produced with $P = P_Y$, where P_Y is the set of subscripts of all the predecessors of *Y*.

2.2 Residual evaluation with the CUSUM method

The CUSUM method is used to evaluate the generated residual signals with respect to its insensitivity to the noise and outliers in the measurements. Moreover, the CUSUM method is able to detect both positive and negative jumps in the mean of the residual signal. The direction of the change provides useful information for fault diagnosis.

The residual signals produced are mapped to the set {0, 1, −1} by the CUSUM method. In the faultless case, the residuals are assumed to be zero mean random signals, and in the case of a fault the mean value of the residual signal is changing in either a positive or a negative direction.

The CUSUM algorithm (Hinckley, 1971) for positive mean jumps is given by the following equations:

$$\sum(k) = \sum(k-1) + \delta(k) - \mu_0 - \beta/2 \quad (4)$$

$$\sum\nolimits_{\min}(k) = \min\left(\sum\nolimits_{\min}(k-1), \sum(k)\right) \quad (5)$$

where β is a user-specified minimum detectable jump, $\delta(k)$ is the residual signals, and μ_0 is the mean value of the nominal signal. Whenever $\sum(k) - \sum\nolimits_{\min}(k) > \lambda$, a jump has been detected. β and λ are design parameters, usually tuned according to the requirements for the false alarm and missed alarm rates. Parameter λ also provides robustness to the fault detection but it also delays the detection. A similar algorithm for the detection of negative mean jumps can easily be obtained by modifying Equations 4 and 5. In the rest of the paper, the result of the CUSUM calculation will be denoted as a function: *CU* ( ).

2.3 Fault isolation reasoning with rules

Fault isolation is performed recursively for the nodes in the detection set by using a set of rules. These isolation rules, developed by Montmain and Gentil (2000), are converted into a table for the convenience of implementation, as shown in Table 1.

After fault isolation, the nature of the fault is identified by testing how the faults propagate to their children nodes. If the fault propagates through the digraph globally, it is identified as a process fault; otherwise it is defined as a local measurement fault. The rules for identifying the nature of the fault are given in Table 2.

Table 1. Fault isolation rules of the dynamic causal digraph

$CU(GR(Y))$	$CU(TLR(Y))$	$CU(ILR_Y(m))$	$CU(ILR_Y(i))$	$CU(MLRY(P_1))$	$CU(MLR_Y(P_2))$	Decision
0	0	0	0	0	0	No fault
1/−1	0	0*	1/−1*	0*	1/−1*	Fault propagates from the parent node *m*
1/−1	0	1/−1**	1/−1**	1/−1**	0**	Fault propagates from the nodes with subscript in P_2
1/−1	1/−1	1/−1	1/−1	1/−1	1/−1	Local fault on variable *Y*

* $\forall i \neq m, i \in P_Y,\ m \in P_1,\ m \notin P_2,\ P_Y$ is the set of subscripts of parents nodes of the node *Y*.

** $\forall i, m, i \in P_Y, m \in P_Y,\ \forall P_1, P_2 \subseteq P_Y$

Table 2. Fault nature rules of the dynamic causal digraph.

$CU(GR(X))$*	$CU(TLR(X))$	Fault nature
1/−1	1/−1	Local fault for that child node
1/−1	0	Process fault for the faulty node
0	1/−1	Measurement fault for the faulty node

**X* is the subscript of any child nodes of the node *Y*.

2.4 Locating the process fault on the arcs

In the case of a process fault, in addition to locating the fault on the variables, locating it on the arcs is also desirable. However, the MISO structure of the digraph causes problems by generating spurious results. In order to decrease the number of spurious results, a new inference mechanism between the arcs is proposed for evaluating the sets of suspected arcs. The idea behind that is to test the consistency between the sets of suspected arcs formed from fault origins and the knowledge of the output arcs from the same node.

The knowledge matrix of the whole digraph is formed by the knowledge matrices of each node which has output arcs. In order to represent this type of knowledge for a node, *U*, in a digraph, the matrix M_U is specified as

$$M_U(i, j) = \begin{cases} 1, \text{ if the inconsistent arc} < U, i > \\ \quad \text{results in the inconsistency} \\ \quad \text{of} < U, j > \\ 0, \text{ otherwise} \end{cases} \quad (6)$$

The dimension of the matrix M_U for node *U* is $n \times n$, if *n* is the number of output arcs which a node has. The knowledge matrix *M* for all the arcs in the digraph model is obtained by merging the knowledge matrices of every individual node in the digraph model, given as:

$$M = \text{blockdiag}(M_1, M_2, ..., M_l) \quad (7)$$

where *l* denotes the number of nodes that have output arcs in the digraph model. The knowledge matrix *M* has the dimension $N_a \times N_a$, where N_a is the number of arcs in the digraph, and each row or column represents one arc in the digraph.

The consistency test between the sets of suspected arcs and the knowledge matrix *M* is performed by matrix manipulation. First, one row vector *SV* with length N_a is formed for one specific set of suspected arcs:

$$SV(i) = \begin{cases} 1, \text{ if } \ ARC(M, i) \in S, 1 \le i \le N_a \\ 0, \text{ otherwise} \end{cases} \quad (8)$$

where *ARC*(*M*, *i*) gives the arc corresponding to the *i*th row in the matrix *M*. The set *S* of suspected arcs is evaluated by multiplying the row vector *SV* and the matrix *M* of the digraph. The set *S* is considered as a possible result only when the number of nonzero entries in the obtained row vector does not change when compared to the row vector *SV*:

$$NUM(SV) = NUM(SV \cdot M) \quad (9)$$

where *NUM*() gives the number of nonzero entries in the matrix.

3. TESTING ENVIRONMENT

The proposed novel casual digraph method was tested on the paper machine short circulation process, which was simulated using the Advanced Process Simulation Environment (APROS) developed by VTT (Technical Research Centre of Finland). A description of the short circulation process and the simulation environment are given in this chapter.

3.1 Description of the short circulation process

The short circulation is a crucial part of the papermaking process, with several important functions. The dilution of the fiber-suspension entering the process to a suitable consistency for the headbox takes place in the short circulation, in a mixing process were low-consistency water from the wire-pit is mixed with high-consistency stock. The second important task of the short circulation is the removal of impurities and air. This task is performed in the hydro-cyclones, machine screens and the so-called deculator. The short circulation also improves the economy of the process because the valuable fibres and filler materials that pass through the wire are recycled. As the intermediate process between stock preparation and former, the short circulation process is very important for paper quality control, since the basic weight, ash consistency and stock jet

ratio control are performed in the short circulation part.

The short circulation process starts after a machine chest. Usually the machine chest is followed by a thick stock pump and a basic weight valve, which is used for basic weight control. The thick stock is pumped to the wire pit and mixed with white water and filler controlled by the filler valve. The diluted stock is pumped by a fan pump via the hydrocyclones to the deculator. The deculator has a continuous overflow to keep the inlet pressure constant for the head box feed pump. The diluted stock is then pumped into the hydraulic headbox and sprayed onto the wire at a constant speed. On the wire the stock is dehydrated to form a wet web. About 98% of the water and 54% of the filler and fibre go through the wire and flow to the wire pit as white water. The process is presented in Figure 1.

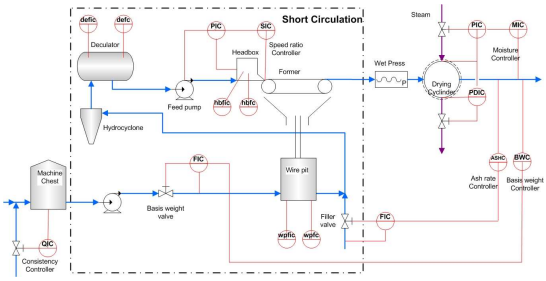

Fig. 1. Flow sheet of the paper machine.

The variables shown in Figure 1 are important for building the causal digraph model. Table 3 gives a description of the variables.

Table 3 Description of the variables in the short circulation

Variables	Description	Unit
baval	Basis weight valve opening	-
wp_fc	Filler consistency in the wire pit	%
wp_fic	Fiber consistency in the wire pit	%
fival	Filler adding valve opening	-
de_fc	Filler consistency in the deculator	%
de_fic	Fiber consistency in the deculator	%
hb_fic	Fiber consistency in the headbox	%
hb_fc	Filler consistency in the headbox	%
feedpump	Headbox feed pump rotation	%
totalflow	Mass flow into the headbox	kg/s
bw	Basis weight of paper	g/m^2
ash	Ash consistency of paper	%

3.2 Simulation environment

The test of the novel dynamic causal digraph method was carried out in the APROS simulation environment. The APROS paper machine simulator provides validated model algorithms for the process components, such as equipment and automation, of the paper machine. These component models are mainly based on first principles. The simulation model is constructed by drawing the process flowsheet and setting up the parameters of the components (Lappalainen, 2003). One built-in paper machine model was provided by VTT for the basic simulation. The control loops were added and the process components were parameterized according to a typical setup of the papermaking process (Paulapuro, 2000; Karlsson , 2000; VTT, 2005). The APROS paper machine model with control loops is shown in Figure 2 and the setups of the pulp recipe, process component parameters, and the grade of the produced paper are given in Table 4.

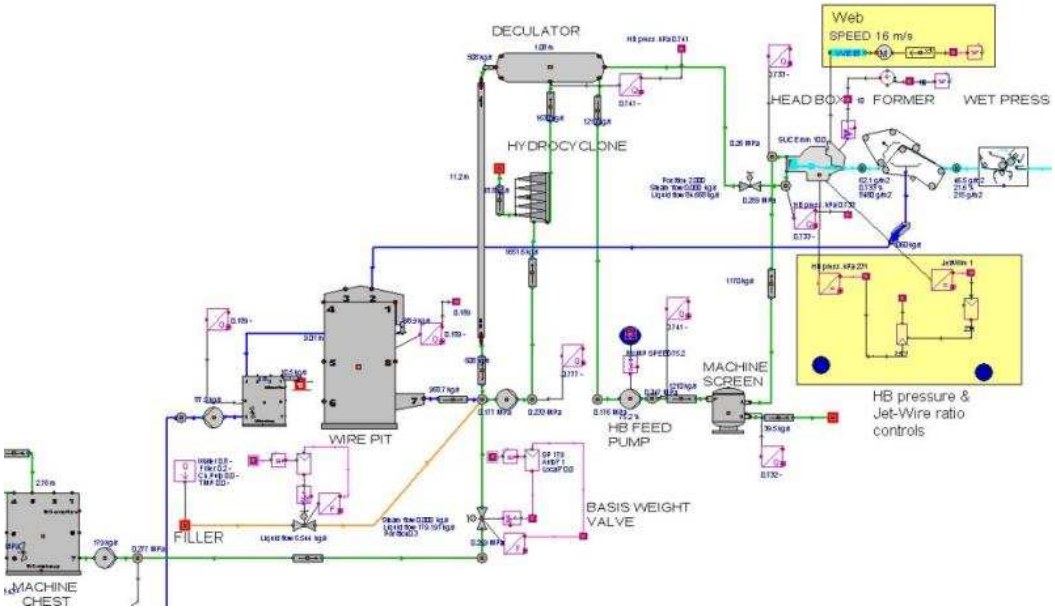

Fig. 2. APROS model for paper machine

Table 4 Setup of the paper machine simulator (Paulapuro, 2000; Karlsson , 2000).

Name	Value	Unit/Description
Pulp recipe (Broke:CP:TMP)	30:21:49	
Fiber retention on wire	58	%
Filler retention on wire	50	%
Number of nips in wet press	3	Type: shoe
Linear pressure on the nips	70,90,120	kN/m
Steam supply pressure for dryer	500	kPa
Web speed	16	m/s
Web width	8	m
Paper basis weight	50	g/m^2
Paper ash rate	18	%
Paper moisture rate	7	%
Basis weight valve nominal pressure drop	30	kPa
Filler weight valve nominal pressure drop	100	kpa

4. CASE STUDIES AND RESULTS

This paper provides three case studies concerning fault detection and isolation on the paper machine short circulation process. The three studied faults are: 1) fiber consistency in the deculator (sensor fault), and 2) filler retention drop on the wire section (process fault). The two fault scenarios, the experimental procedures and the results for each fault scenario are presented in the remainder of this section.

4.1 Fault scenarios

Three different types of fault were introduced into the APROS paper machine model in sequence in order to test the proposed method. The first fault introduced was a measurement fault on the fiber consistency in the headbox. A drift fault with a slope of $3.5e^{-6}$%/s was added to the fault-free measurement *de_fic*.

The second fault introduced was a process fault, in which the filler retention on the wire dropped. In the APROS model the fault was simulated by changing the retention setup for filler from 45% to 40%. Because of the smaller size of the filler compared to the fibers in the stock, the retention rate for the filler is relatively low. The decrease in the filler retention will directly affect the ash rate of the final paper. Although the quality control for the ash rate maintained the paper quality following the setpoint, the paper machine was running inefficiently. Furthermore the filler transportation ability was affected considerably. Moreover, since it is difficult to transfer filler to the final product, it will accumulate in the short circulation, which increases the wear of process devices like pumps, pipes and valves. As a result of the above, a filler retention drop fault can cause serious problems that require as early as possible detection and identification.

4.2 Description of the experiment

The case studies on the short circulation process were carried out in 3 steps. First the linearity of the paper machine process was tested in an open loop in order to evaluate whether linear state-space models can accurately describe the process behaviour. The structure of the causal digraph model was also decided in this phase, as shown in Figure 3. The result of the test according to the digraph structure indicated that the paper machine model used by APROS is relatively linear when the paper grade defined in Table 4 was produced.

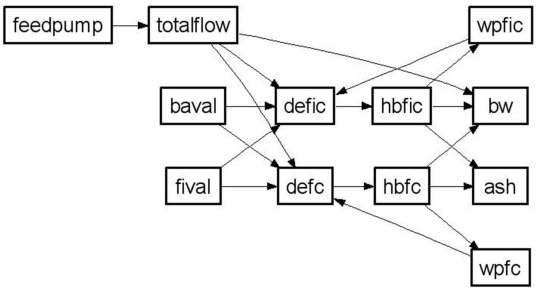

Fig.3. Causal digraph model for the short circulation process.

Secondly, the simulation in an open loop was run for modelling the cause-effect relationships in the digraph, during which the basis weight valve, filler valve and feed pump for the headbox were adjusted manually. The discrete-time state space models for the causal digraph model were identified by training the recurrent neural networks with linear nodes only. The NNDT software was used for the training task (Saxén, 1994).

The last step of the experiment was to run the simulation with the control loops closed. In this phase, two different artificial faults were introduced into the APROS model and the proposed method was applied to detect and identify the faults. The total simulation time was 25800 seconds (about 7.2 hours), and the sampling time was 10 seconds. The two faults were introduced into the simulator in

sequence at the time intervals 1800−7800 s and 8800−17800 s respectively

4.3 Diagnosis results for the fault on the sensor of fiber consistency in deculator

The first faulty scenario is a measurement fault for the fiber consistency in the deculator. It was simulated during the time period 1800−7800 s. The *GR*s shown in Figure 4 indicate that, during this time period, only the variable *de_fic* produced an alarm. The fault isolation rules clearly infer that the fault is local, and the fault nature rules infer that it is a measurement fault. Finally, the fault propagation path for the time period (1800−7800 s) is shown as the fault diagnosis result in Figure 5.

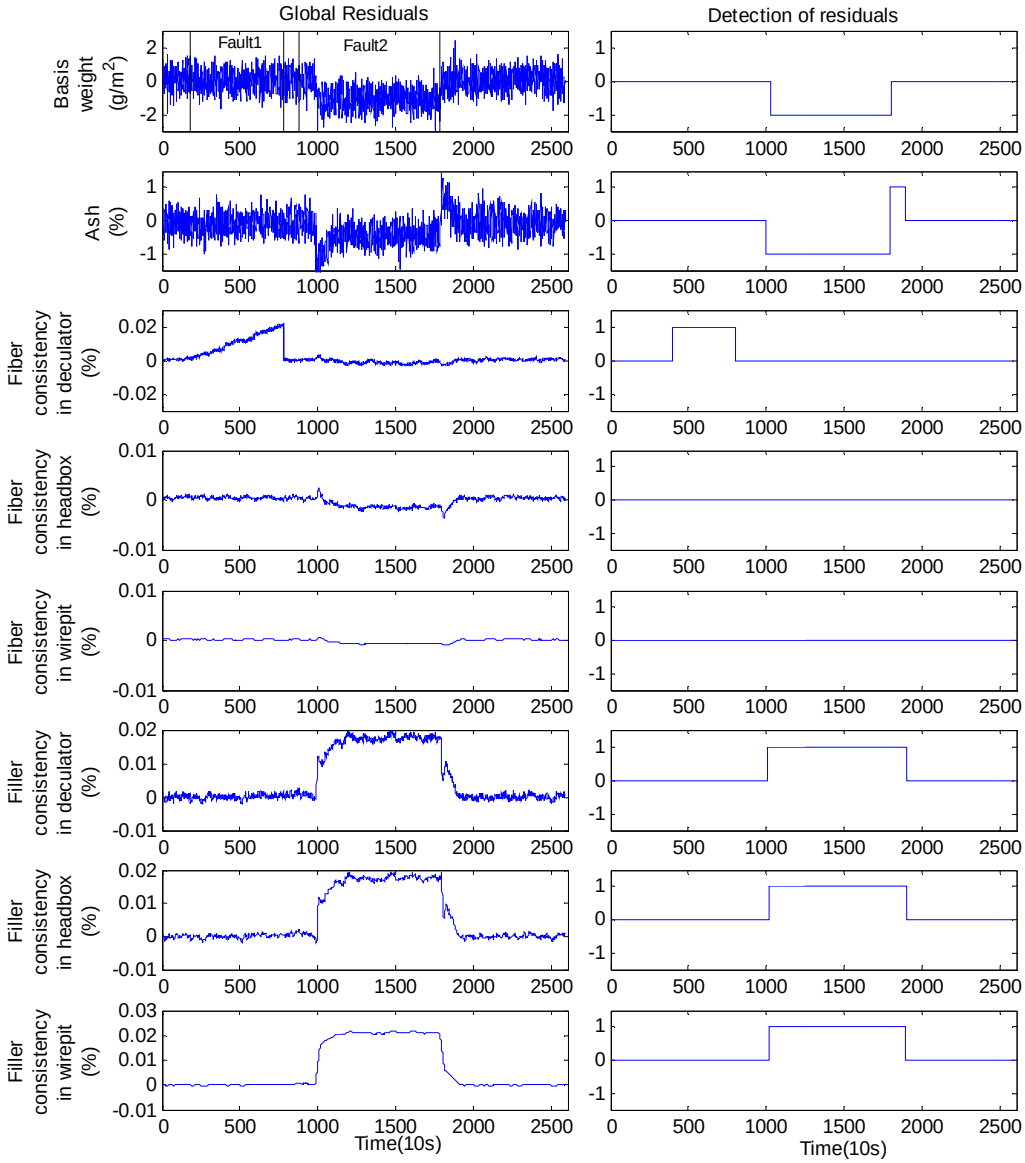

Fig. 4. Global residuals for the variables *bw*, *ash*, *de_fic*, *hb_fic*, *wp_fic*, *de_fc*, *hb_fic and wp_fc*.

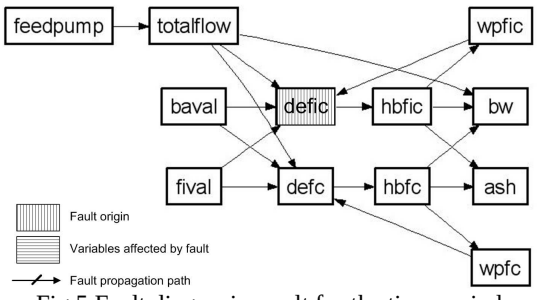

Fig.5 Fault diagnosis result for the time period 1800−7800 s.

4.4 Diagnosis results for a filler retention drop on the wire section

The third fault scenario is a retention drop of filler on the wire section, which can be characterized as a process fault. The fault was simulated during the time period 17800−25800 s. The variables *ash*, *bw*, *de_fc*, *wp_fc* and *hb_fc* were detected from the *GR*s shown in Figure 4 for the period 8800− 17800 s, and the detection set was formed. *LR*s are generated for the variables in the detection set and fault isolation rules are applied. . As the final fault diagnosis result, the fault propagation path is formed as shown in

Figure 6, where all the variables in the detection set have been processed.

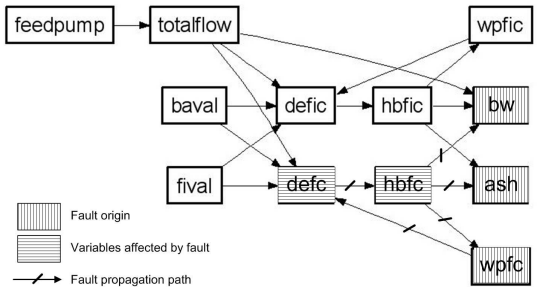

Fig.6 Fault diagnosis result for the time period 8800−17800 s.

The fault was identified as a process fault by the fault nature rules because the fault propagated globally through the digraph. Location of the process fault is performed in order to find the responsible process component. However, spurious results were produced due to the multiple fault origins and multiple input arcs for each fault origin. In Figure 6 the input arcs for fault origin nodes *wp_fc*, *bw*, *ash* are {<*hb_fc*, *wp_fc*>}, {<*totalflow*, *bw*>, <*hb_fic*, *bw*>, <*hb_fc*, *bw*>} and {<*hb_fic*, *ash*>, <*hb_fc*, *ash*>}, respectively. Thus the number of sets of suspected arcs is $1\cdot(2^2-1)\cdot(2^3-1)=21$, which are {<*hb_fc*, *wp_fc*>, <*totalflow*, *bw*>, < *hb_fc*, *ash*>}, {<*hb_fc*, *wp_fc*>, <*hb_fic*, *bw*>, <*hb_fic*, *ash*>}…

In order to perform the inference between arcs, knowledge about the relationship between the output arcs was introduced into the digraph model. The knowledge matrix *M* for the digraph is formed by the knowledge matrix of each node that has output arcs:

$$
\begin{aligned}
&M_{feedpump}=1;\ M_{totalflow}=\begin{bmatrix}1&0&0\\0&1&1\\0&1&1\end{bmatrix};\\
&M_{baval}=\begin{bmatrix}1&0\\1&1\end{bmatrix};\ M_{fival}=\begin{bmatrix}1&1\\0&1\end{bmatrix};\ M_{defic}=1;\\
&M_{defc}=1;\ M_{hbfic}=\begin{bmatrix}1&1&1\\1&1&1\\1&1&1\end{bmatrix};\ M_{hbfc}=\begin{bmatrix}1&1&1\\1&1&1\\1&1&1\end{bmatrix};\\
&M_{wpfic}=1;\ M_{wpfc}=1\\
&M=\text{blockdiag}\begin{pmatrix}M_{feedpump},M_{totalflow},\\M_{baval},M_{fival},M_{defic},\\M_{defc},M_{hbfic},M_{hbfc},\\M_{wpfic},M_{wpfc}\end{pmatrix}
\end{aligned}
\tag{10}
$$

The corresponding arcs represented by each row of the matrix *M* are:<*feedpump*, *totalflow* >, < *totalflow*, *bw*>, <*totalflow*, *de_fic*>, <*totalflow*, *de_fc*>, <*baval*, *de_fic*>, <*baval*, *de_fc*>, <*fival*, *de_fic*>, <*fival*, *de_fc*>, <*de_fic*, *hb_fic*>, <*de_fc*, *hb_fc*>, <*hb_fic*, *wp_fic*>, <*hb_fic*, *bw*>, <*hb_fic*, *ash*>, <*hb_fc*, *bw*>, <*hb_fc*, *ash*>, <*hb_fc*, *wp_fc*>, <*wp_fic*, *de_fic*>, <*wp_fc*, *de_fc*>.

The knowledge included in the matrix *M* is based on process knowledge from paper machines. The sub matrix $M_{totalflow}=\begin{bmatrix}1&0&0\\0&1&1\\0&1&1\end{bmatrix}$ represents the relationship between the arc <*totalflow*, *bw*>, <*totalflow*, *de_fic*> and <*totalflow*, *de_fc*>. It can be seen from matrix $M_{totalflow}$ that the inconsistency of arc <*totalflow*, *bw*> does not result in an inconsistency of other output arcs, since the arc <*totalflow*, *bw*> represents the cause-effect relationship between the mass flow through the headbox and the basis weight variable of the paper, and the arcs <*totalflow*, *de_fic*> and <*totalflow*, *de_fc*> are located before the headbox in the process. It can also been seen from matrix $M_{totalflow}$ that whenever one of the arcs <*totalflow*, *de_fic*> and <*totalflow*, *de_fc*> is faulty, then the other one is also faulty. This is based on the fact that, in the process, the relationship between mass flow through the headbox and the fiber consistency in the deculator is correlated with the relationship between the mass flow and the filler consistency in the deculator, since they physically share the same pipe from the deculator.

The sub matrix $M_{baval}=\begin{bmatrix}1&0\\1&1\end{bmatrix}$ represents the relationship between the arc <*baval*, *de_fic*> and <*baval*, *de_fc*>. Theoretically, if the actuator fault in the basis weight valve causes the inconsistency of <*baval*, *de_fic*> or <*baval*, *de_fc*>, then another arc should be faulty at the same time, since the relationship between the control signal and the mass flow through the basis weight valve changed due to the fault, thus subsequently changing the relationship on the arc <*baval*, *de_fic*> and <*baval*, *de_fc*>. However, the dilution effect represented by the arc <*baval*, *de_fc*> is so small that the fault on it cannot always produce residuals on the node *de_fc* that are large enough for detection when the fault on arc <*baval*, *de_fic*> produces large enough residuals for detection. On the other hand, if the fault on arc <*baval*, *de_fc*> is significant enough to detect, then the fault on <*baval*, *de_fic*> must be significant enough for detection. Based on the above, the noncommutative matrix $M_{baval}=\begin{bmatrix}1&0\\1&1\end{bmatrix}$ is used to represent the knowledge between arc <*baval*, *de_fic*> and <*baval*, *de_fc*>. For the same reason, the matrix $M_{fival}=\begin{bmatrix}1&1\\0&1\end{bmatrix}$ is used to represent the knowledge between arc <*fival*, *de_fic*> and <*fival*, *de_fc*>.

The sub matrix $M_{hbfc}=\begin{bmatrix}1&1&1\\1&1&1\\1&1&1\end{bmatrix}$ represents the relationship between arc <*hb_fc*, *bw*>, <*hb_fc*, *ash*> and <*hb_fc*, *wp_fc*>. This sub matrix is obtained from the knowledge of the filler material balance. Whenever the filler flows to the wire pit decrease or increase, the filler flows to final production (*ash* and *bw*) increase or decrease. The same matrix

$M_{hbfic} = \begin{bmatrix} 1 & 1 & 1 \\ 1 & 1 & 1 \\ 1 & 1 & 1 \end{bmatrix}$ is obtained for the arcs <*hb_fic*, *bw*>, <*hb_fic*, *ash*> and <*hb_fic*, *wp_fc*>.

With the knowledge matrix *M* given in Equation 10, the 21 sets of suspected arcs were tested with Equation 9. The set of suspected arcs {<*hb_fc*, *wp_fc*>, <*hb_fic*, *ash*>, <*hb_fic*, *bw*>} is considered as an example. The *SV* for this set is

$$SV = [0\ 0\ 0\ 0\ 0\ 0\ 0\ 0\ 0\ 0\ 0\ 1\ 1\ 0\ 0\ 1\ 0\ 0] \quad (11)$$

and the test with Equation 9 is performed as follows:

$$NUM(SV) = 3 \neq NUM(SV \cdot M) = NUM([0\ 0\ 0\ 0\ 0\ 0\ 0\ 0\ 0\ 0\ 2\ 2\ 2\ 1\ 1\ 1\ 0\ 0]) = 6 \quad (12)$$

Thus the set {<*hb_fc*, *wp_fc*>, <*hb_fic*, *ash*>, <*hb_fic*, *bw*>} cannot be a possible result. The set {<*hb_fc*, *wp_fc*>, <*hb_fc*, *ash*>, <*hb_fc*, *bw*>} is considered as another example. The SV for the set is

$$SV = [0\ 0\ 0\ 0\ 0\ 0\ 0\ 0\ 0\ 0\ 0\ 0\ 0\ 1\ 1\ 1\ 0\ 0] \quad (13)$$

and the test with Equation 9 is performed as follow:

$$NUM(SV) = 3 = NUM(SV \cdot M) = NUM([0\ 0\ 0\ 0\ 0\ 0\ 0\ 0\ 0\ 0\ 0\ 0\ 3\ 3\ 3\ 0\ 0]) = 3 \quad (14)$$

Thus this set is accepted as a possible result. After the test of all the sets of suspected arcs, only two were left as possible results: {<*hb_fc*, *wp_fc*>, <*hb_fc*, *ash*>, <*hb_fc*, *bw*>} and {<*hb_fc*, *wp_fc*>, <*hb_fc*, *ash*>, <*hb_fc*, *bw*>, <*totalflow*, *bw*>}. The number of possible results decreased from 21 to 2 by using the inference mechanism between arcs.

The fault diagnosis results, i.e. the two sets of suspected arcs, provide valuable information in identifying the faulty process component in the case of a process fault. The first arc in the first set {<*hb_fc*, *wp_fc*>, <*hb_fc*, *ash*>, <*hb_fc*, *bw*>} is <*hb_fc*, *wp_fc*>, which corresponds to the process components: a wire section and the white water tray. Similarly, the arcs <*hb_fc*, *ash*> and <*hb_fc*, *bw*> correspond to the process components: a wire section, a wet press and a drying group. Thus the suspected process component is the wire section, since it is located on all three arcs. The same result is obtained from the second set. Moreover, the results also indicated that the fault occurred for the filler material but not for the fiber material. Finally, the direction of the GR(*wp_fc*), as shown in Figure 4, implies that the direction of the fault is the drop in the filler retention, rather than an increase in the filler retention.

In this fault scenario, the fault effects separation approach was applied to locate correct fault origins; with the inference mechanism between arcs, the number of the possible fault results decreased significantly and the process fault was located on the arcs, which subsequently helps to identify the faulty process component, i.e. a wire section. The example of this fault scenario illustrates the necessity and the power of the modified dynamic causal digraph for industrial applications.

5. CONCLUSIONS

An enhanced dynamic causal digraph reasoning method for fault diagnosis in a paper machine short circulation process was presented in this paper. The capacity to handle process faults were improved with the inference mechanism between arcs by locating the process fault on the arcs. Two different fault scenarios were tested with the proposed method in a paper machine short circulation process: a sensor fault and a process fault. The results for the first scenario, i.e. a sensor fault, showed that the conventional dynamic causal digraph was able to handle this case well. In the second scenario, the fault diagnosis result was improved further by locating the process fault on the arcs using the proposed inference mechanism, and more information was provided by the novel method, which can identify the faulty process component.

ACKNOWLEDGEMENTS

This work is finically supported by the Finnish Funding Agency for Technology and Innovation.

REFERENCES

Fagarasan, I., S. Ploix and S. Gentil (2004) Causal fault detection and isolation based on a set-membership approach, A*utomatica*, **40** pp. 2099-2110.

Hinckley, D.V. (1971). Inference about the change-point from cumulative sum tests, *Biometrika*, **58**, pp. 509-523.

Iri, M., K., Aoki, E., O'Shima and H., Matsuyama (1979). An algorithm for diagnosis of system failures in the chemical process, *Computer & Chemical Engineering*, **3 (1-4)**, pp.489-493

Karlsson, M. (2000) Papermaking Part 2, drying, Papermaking Science and Technology Book 9, Fapet Oy, Jyväskylä, Finland, 242p.

Lappalainen, J., T. Myller, O. Vehviläinen, S. Tuuri and K., Juslin (2003) Enhancing grade changes using dynamic simulation, *TAPPI Journal*, **2 (12)**.

Leyval, L., S. Gentil and S., Feray-beaumont (1994). Model-based Causal Reasoning for Process Supervision, *Automatica*, **30**, pp. 1295-1306

Montmain, J. and S., Gentil (2000). Dynamic causal model diagnostic reasoning for online technical process supervision, *Automatica*, **36**, pp. 1137-1152

Paulapuro, H. (2000) Papermaking Part 1, Stock Preparation and wet end, Papermaking Science and Technology Book 8, Fapet Oy, Jyväskylä, Finland, pp. 131-136p, 297p.

Saxén B. and H., Saxén (1994). NNDT - A neural network development tool - User's guide, Technical Report 94-8, Heat Eng. Lab, Åbo Akademi University, Åbo.

Shih R. and L. Lee (1995). Use of Fuzzy Cause-Effect Digraph for Resolution Fault Diagnosis for Process Plants. 1&2. Fuzzy Cause-Effect Digraph, *Industrial & Engineering Chemistry Research*, **34**, pp. 1688-1717.

VTT(2005), APROS 5.0.4 help document, VTT, Espoo, Finland, 2005.